ACTA IMEKO
ISSN: 2221-870X
June 2025, Volume 14, Number 2, 1 - 9

A wireless, inertial measurement unit-based sensing architecture for detecting geomorphological landslides

Marcel Musuamba[1], Aimé Lay-Ekuakille[1], Trésor Auguste Mafuku[1], Benjamin Kalala[1]

[1] *Electronic and automation Laboratory, Institut Supérieur Pédagogique et Technique de Kinshasa, ISPT-Kin. Av. De la science, n°5, Gombe-Kinshasa, DR Congo*

ABSTRACT
Landslide activities must be monitored by means of robust sensing and acquisition systems in the spirit of quick intervention in the event of stealth and/or huge subsoil displacements. Acquiring diverse parameters, in order to address this issue, is an important area of research. This paper illustrates a case-study with a dedicated architecture. The multiparametric acquisition system is developed to acquire in real time data related to linear and rotational displacement parameters. These data are used to prevent prospective ground movement. The principal advantage of the implemented system dwells in its flexibility, efficacity, and its transmission speed, as well as its low implementation cost. The sensor planted on site permanently sends these following parameters: acceleration related to the auscultated site, the sensor rotation velocity and the site ambient temperature. These three parameters essentially permit the monitoring of the site state, the sensor position and the site temperature. In this paper, tests are achieved in laboratory simulating two phenomena on which are based our studies: subsidences and collapses.

Section: RESEARCH PAPER

Keywords: Landslide; IMU sensor; wireless and geomorphological acquisition; multiparametric measurements; cloud database

Citation: M. Musuamba, A. Lay-Ekuakille, T. A. Mafuku, B. Kalala, A wireless, inertial measurement unit-based sensing architecture for detecting geomorphological landslide, Acta IMEKO, vol. 14 (2025) no. 2, pp. 1-9. DOI: 10.21014/actaimeko.v14i2.1787

Section Editor: Laura Fabbiano, Politecnico di Bari, Italy

Received February 20, 2024; **In final form** May 18, 2025; **Published** June 2025

Corresponding author: Josué Marcel Musuamba, e-mail: josuemarcelmusuamba7@gmail.com

1. INTRODUCTION

Based on the caused damages criteria, the ground movements are classified as the seventh of the major natural risks (after seism, cyclones or flood) [1], [2]. They are unpredictable as all-natural catastrophe and depend on predisposing factors namely: steep slope in mountains [3], seismicity [4], high intensities of recurring rainfalls [5] and thus they are sources of a lot of damage, hence, needing adequate and effective preventive solutions in order to minimize ground displacements consequences.

The unpredictability of when landslides are likely to occur, makes their consequences more dangerous [6], [7], and they generally impact in slope, catchment or regional scales. [8].

In order to save people from the dangers named above, a particular solution is to alert people for an imminent landslides arrival in a suspected terrain; to achieve this goal, a set of sensors and technologies is implemented, such as: rain gauges, ultrasonic sensors, seismic sensors, tensiometers, piezometers, extensometers, various meteorological sensors etc. are used to assess the landslide hazards based on several parameters. [8].

To acquire the soil characteristics or parameters, and to understand every involved parameter, one uses different kinds of devices, and techniques that handle various technologies, as well as requirements for the acquisition tools implemented [9]. The study quality, that is, the accuracy of the results, and the implemented system efficiency for prevention, is deeply related to the employed material qualities requiring a lot of implementation means; that constitutes one of the obstacles when solving natural disasters prevention problem. Thanks to progress in prevention of some natural disasters such as seism, tsunami, …, it is now possible to use techniques used in seism prevention or other ground disaster and apply them to control the sites under risk of landslides in order to generate alert preventing potential ground movement arrival.

The ground movements consist of a ground block displacement (rocky or sandy), controlling permanently these blocks velocities and accelerations, allows to get accurate information of a prospective ground movement.

The landslide and thus the ground movement, can be monitored with seismic networks such as:

- Accelerometric network and alarm system: equipped with a 3-component Kinemetrics EpiSensor accelerometer, connected to a Kinemetrics Granite digital datalogger; [10]
- Seismic Navigating System (SNS) array based on the nanoseismic monitoring technique. [10].

The choice of the system, to be implemented, is related to activities held in the site, for example for Seismic monitoring of building, in this case the system allows remote control, and remote and real-time monitoring of the building vibration. [11]. Or, for the ground behaviour monitoring in underground mines. [12].

In [13], the capabilities and limitations of satellite InSAR and terrestrial radar interferometry techniques are described, that is for example these systems are only capable of measuring the deformation occurring in the line of sight of the system; and theirs costs make that such systems are difficult to be used by everyone in need.

In [14], the D-InSAR method was used to monitor landslides located in Savoie (France), this study showed several points:

- Accurate study with DEM (Digital Elevation Model) is very important to limit the processing errors;
- The conditions of the atmosphere can cause a wave diffraction. So, the D-InSAR could be incorrect.

So, in this paper, we are building a wireless device based on the multiparametric IMU (Inertial Measurement Unit) sensor, containing the accelerometer, the gyroscope and the temperature sensor, and intend to show its application in a wireless network system for the landslide prediction or prevention. And how the acquired data could be used when performing a machine learning project for the prevention of ground movement.

Nowadays, there is a panoply (or range) of sensors dedicated to each movement type [15], and various implementing technologies. Thus, for the monitoring of site susceptible to landslides risk. The use of:

- An embedded triaxial accelerometer allows to acquire on real time the accelerations values according to the three axes;
- The accelerograms allow to characterize the site state, and a dataset of several signals retrieved from others ground movement can lead up to generate predictions;
- An algorithm implemented must allow the alerts generations from a determined acceleration threshold;
- A gyroscope to determine the sensor rotational velocities according to the three axes;
- An internet connection to allow data to be sent to the cloud database by the sensors, and their retrieval by the processing systems in order to process data and generate the alerts.

The architecture thus built, should allow to monitor the sites and prevent the eventual movements. That is confirmed by the tests result based on the simulated collapse and subsidence in the case of our study.

To achieve our goal, this paper is structured in the following way, a part from the introduction (section 1) and the conclusion (section 5): In section 2, we have proposed a literature related to the problem of the ground displacement detection, and have shown the limits, as well as, constraints of the more used process till now; In section 3, we have described the architecture implemented to handle the experiments, and the characteristics of the used devices; In section 4, results are presented, and analyzed with reference to data processing procedures. Conclusions, and future work end the paper.

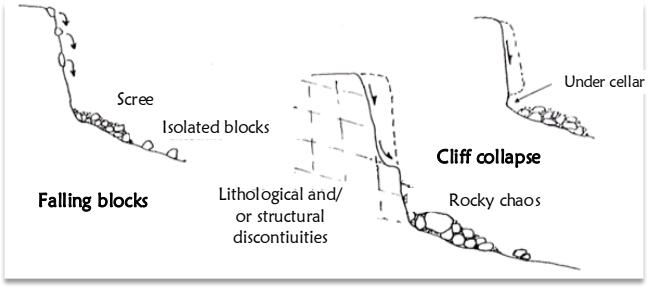

Figure 1. Some ground displacement.

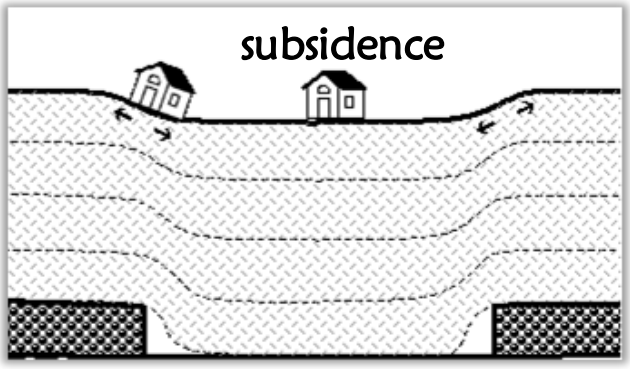

Figure 2. Cross-section of a subsidence phenomenon.

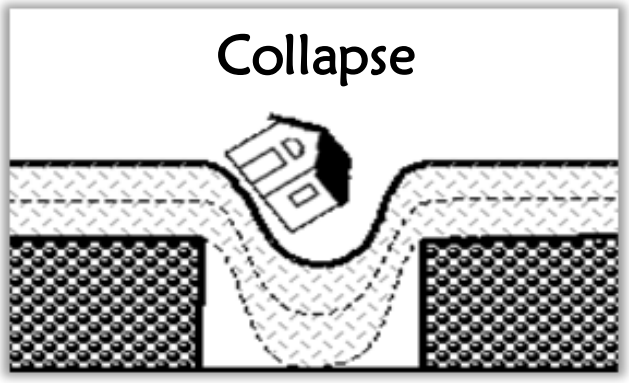

Figure 3. Cross-section of a collapse phenomenon

2. GROUND DISPLACEMENT DETECTION

The ground movement designates soil, and subsoil displacements, more or less brutal, under natural effect influences: heavy precipitations, alternating freeze, and thaw, erosion, etc. or anthropogenics: materials exploitation, deforestation, earthwork, etc. [16].

- Subsidences are bowl-shaped topographical depressions due to the slow, and progressive sagging of the overlying terrain [16];
- Collapse results from the breakdown of supports or the superior part of an underground cavity [16].

These ground movements are likened to all other natural damages (seism, tsunami, volcano, …), which go with vibrations movements spreading in all directions around the soil. That is elastic wave because inducing reversible general deformations [17].

One can distinguish thus two types of seismic waves:

- *Body waves* traveling through the inner part of the earth, and in an independent manner. Their propagation velocity depends on the material crossed and increases with the depth. We distinguish: *Primary wave (P-wave), and Secondary wave (S-wave)* which are respectively longitudinal wave or compressional wave (with a velocity of 7 to 8 km·s^{-1}around the surface), and the *shear wave* (with a velocity of 4 to 5 km·s^{-1} around the surface) [17], see Figure 4.
- *Surface waves* generated by the interaction of the P and S waves. They can be divided into two types: *Love waves,* and *Rayleigh waves* [17]. It is illustrated in Figure 5.

These waves, when detected, can be plotted in accelerograms as shown in Figure 6 on which we indicate the different types of seismic waves

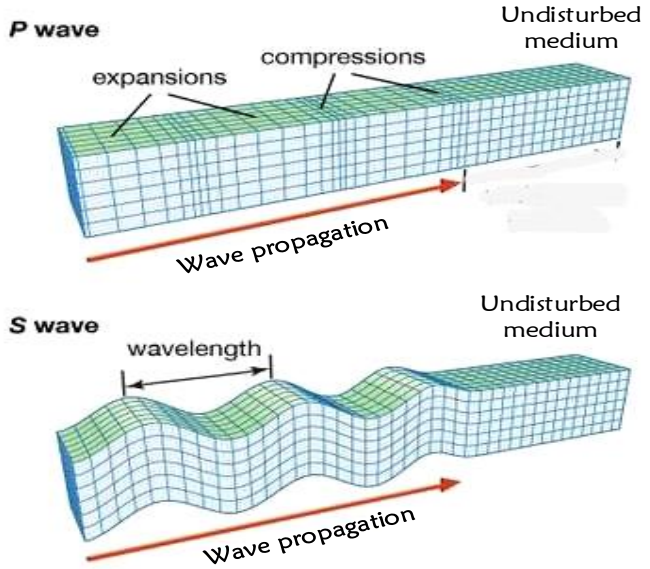

Figure 4. Illustrating the body wave.

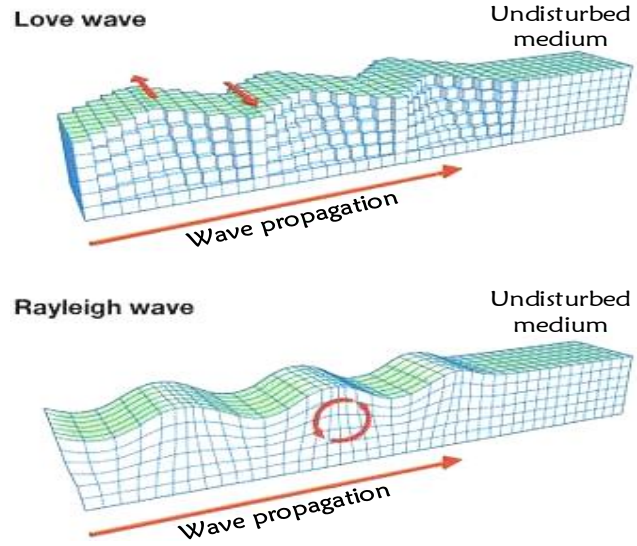

Figure 5. Illustrating the surface wave

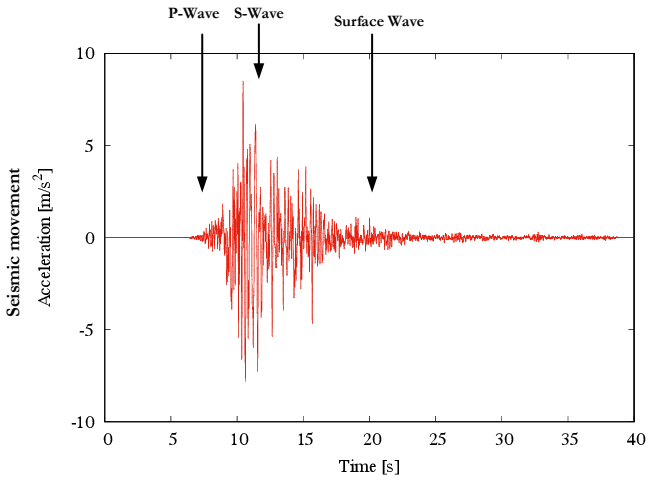

Figure 6. Capacitance technique with contact method.

Several techniques can be used to detect such movements, namely:

- *Passive seismic monitoring* which has been validated ten years ago, for unstable blocks about thousand to hundred thousand cubic meters and in different contexts [18]; it consists in: the rocks blocks unstable preferentially vibrate at certain frequencies that are characteristic: of their geometry, their mass, their rock rigidity, but also of their attachment degree to the stable rock masses. Thanks to the seismometers, it is possible to record these frequencies, and even to follow their evolution over time [19].
- *Radar interferometry* [20] consists in comparing the phase of signals acquired at different times, distance variations between two or more acquisitions that are small fractions of the transmitted wavelength can be retrieved. The employed radar works at a center frequency of 17.2GHz (the Ku band, that is, a wavelength of 1.74 cm in vacuum); under the best measurement conditions, a sensitivity of a few microns can be achieved. The main limitation of this interferometric technique is that only the displacement variation along the line of sight (LOS) direction can be achieved. The accuracy of the retrieved displacement depends on the intensity of the radar return. This method is less complete than the passive seismic monitoring with 3 axes seismometers and is complementary thus it allows to monitor cliff vibration by remote sensing, that is very easy to deploy seismometers [21].
- *Satellite radar interferometry* aims to produce the interferograms giving the displacement related to the radar line of sight (LOS). The SAR interferometry is adapted to measure the vertical component of the movement (the satellite pictures site from the top), while the GBSAR interferometry is adapted to measure the horizontal component of the movement (the radar is installed in front of the unstable site) [22]. The method has as limitations sensor spatial resolution less expanded for the displacements (some pixels), and the measures repetitiveness (delay between acquisitions).

3. CONTACT METHOD

For this study, we choose the use, on the one hand, of the IMU based sensor: GY-521 MPU 6050 sensor (Figure 7)

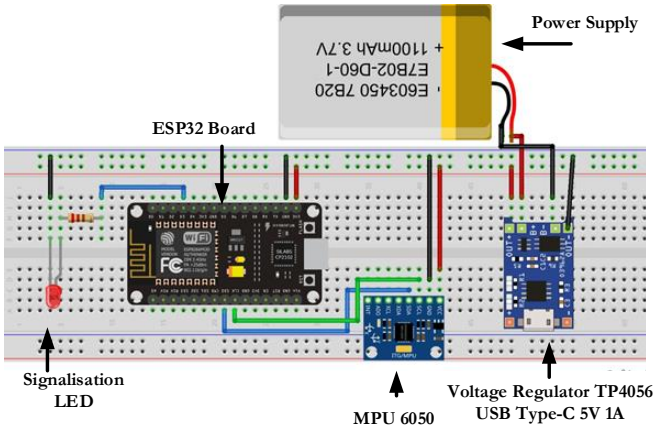

Figure 7. Acquisition hardware system.

constituted of: a 3-axis gyroscope, 3-axis accelerometer, an on-chip temperature sensor and an onboard digital motion processor (DMP); with features:

For the triple-axis MEMS gyroscope:

- User-programmable full-scale range of $\pm 250°/s, \pm 500°/s, \pm 1000°/s,$ and $2000°/s$
- Integrated 16-bit ADCs enable simultaneous sampling gyros
- Operating current: 3.6 mA
- Standby current: 5 µA.

For the triple-axis MEMS accelerometer:

- Full scale range of ± 2 g, ± 4 g, ± 8 g and ± 16 g
- Integrated 16-bit ADCs enable simultaneous sampling of accelerometers while requiring no external multiplexer
- Normal operating current: 500 µA
- Low power accelerometer mode current: 10 µA at 1.25 Hz, 20 µA at 5 Hz, 60 µA at 20 Hz, 110 µA at 40 Hz.

Additional features:

- VDD supply voltage range of $2.375\ V - 3.46\ V$
- 3.9 mA operating current when all 6 motion sensing axes and the DMP are enabled
- Digital output temperature sensor
- 1024 byte FIFO buffer reduces power consumption.

Together, via an I2C connection [23], with the esp32 GSM microcontroller which allows the conditioning of the acquired signals, and assumes the data transfer to the cloud database (for sake of experimentation we use the firebase real-time database interface), and also the sensor power supply. The whole hardware acquisition system is presented in Figure 7.

On the other hand, a PC on which we retrieve the data from the cloud database, and proceed on processing, namely: acceleration threshold detection in order to generate prospective alerts, signals visualization, local data storage, and many other processing to which these signals can be subjected. We use mainly the python programming language, and all the libraries offered. The simplified architecture is shown in Figure 8.

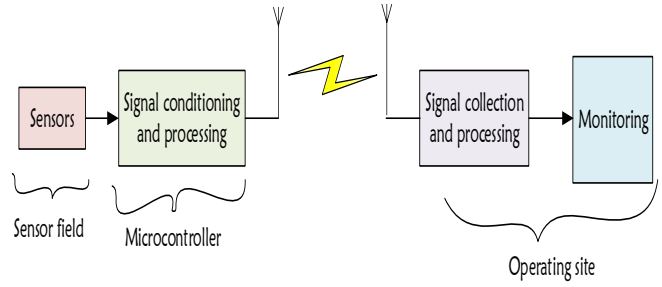

Figure 8. Wireless data acquisition system.

The accelerometer acquisition principle is based on the detection of accelerations according to three axes X, Y, Z that is: $a_x, a_y,$ and a_z in m/s^2 allowing to determine different rotations angles [24], [25]:

- Pitch angle θ

$$\theta = \arctan\frac{a_x}{\sqrt{a_y^2 + a_z^2}} \quad (1)$$

- Yaw angle ρ

$$\rho = \arctan\frac{\sqrt{a_x^2 + a_y^2}}{a_z} \quad (2)$$

- Roll angle φ

$$\varphi = \arctan\frac{a_y}{\sqrt{a_x^2 + a_z^2}}. \quad (3)$$

And the gyroscope allows to measure the rotation velocity around every individual axis, which amounts to the rotation velocity in degree per second ("deg/s" or ("°/s").

We summarize the whole system working principle by the flowchart of the Figure 9.

4. RESULTS ILLUSTRATIONS

Experimentations are carried out on three stages, using a soil sample, and these stages are described as follows:

To achieve these experimentations, we have built a box with a sample of ground, as shown in the Figure 13 (left) where we have put the sensor. So, for the non-event situation in Figure 13 (left) the box was still and no vibration. For the collapse situation

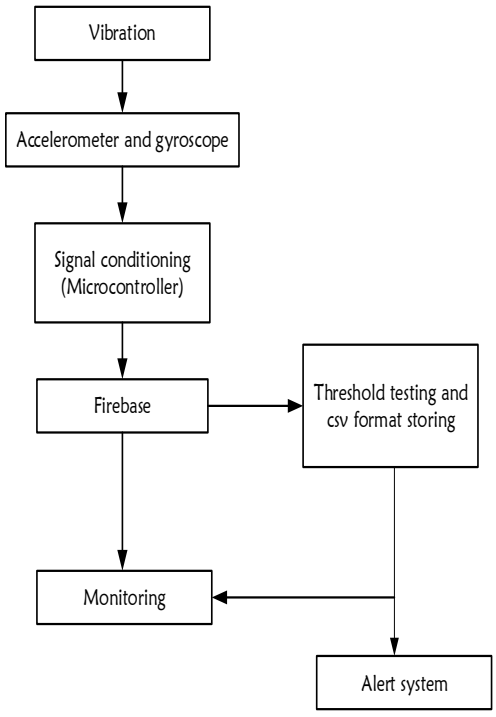

Figure 9. System flowchart.

in Figure 13 (central) with two samples, one used as floor where the sensor is buried and another as removable in a way to simulate the collapse phenomenon by pulling it up and let the ground that it was keeping in a way to generate a vibration on the floor according to the Figure 3. And for the subsidence phenomenon in Figure 13 (right), we have two removable walls that we pull up simultaneously to let the ground, kept from either side, fall on the floor according to the Figure 2.

- **Acceleration data extracted for the non-event**[1]

The non-event experience is when there is not any ground vibration and in this case the yielded accelerograms are as plotted in the figure below, where in blue we have x axis component which has as magnitude about $10\ m/s^2$ that is the gravitation acceleration; the orange and the green are respectively the y-axis and z-axis accelerations and are about zero.

Data for this experience are built in a dataset of four features:

- the timestamp (s): that is the time in seconds when the data were acquired
- the accX (m/s²): is the acceleration according the x-axis data, that we have considered as the vertical axis according to the sensor position
- the accY (m/s²): the accelerations according to the y-axis
- the accZ (m/s²): the acceleration according to the z-axis.

A sample of this dataset is described in Table 1.

- **Acceleration data extracted for the collapse simulation**

A sample of this dataset is described in Table 2.

- **Acceleration data extracted for subsidence simulation**

A sample of this dataset is described in Table 3.

All these data are acquired from the simulated phenomena in Figure 13 and can be plotted following Figure 10, 11 and Figure 12 above.

It is necessary to mention that the data were acquired under some conditioning configuration: the calibration of MPU6050

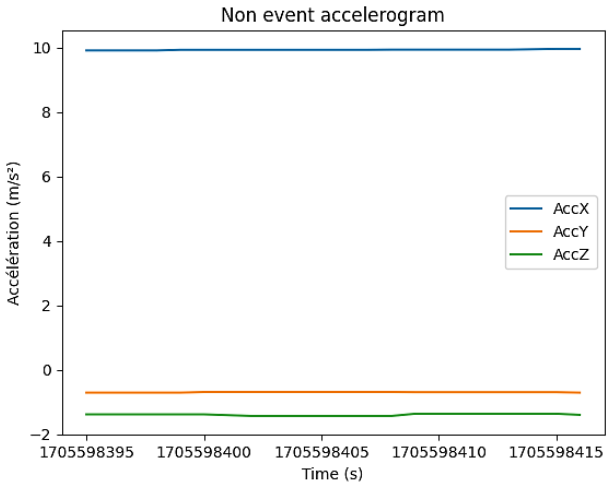

Figure 10. Non-event accelerogram plot.

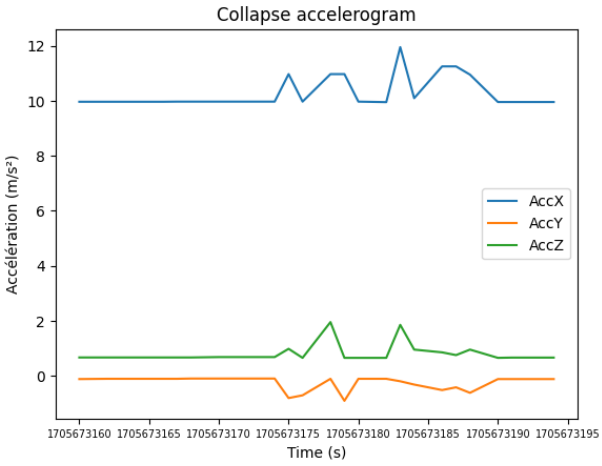

Figure 11. Collapse accelerogram.

Table 1. Non-event dataset sample.

N°	Timestamp in s	accX in m/s²	accY in m/s²	accZ in m/s²
0	1705598395	9.91199	-0.71347	-1.38864
1	1705598396	9.91199	-0.71347	-1.38864
2	1705598398	9.91199	-0.71347	-1.38864
3	1705598399	9.93115	-0.71347	-1.38864
4	1705598400	9.93115	-0.69432	-1.38864
5	1705598402	9.93115	-0.69432	-1.43652
6	1705598403	9.93115	-0.69432	-1.43652
7	1705598404	9.93115	-0.69432	-1.43652
8	1705598406	9.93115	-0.69432	-1.43652
9	1705598407	9.93115	-0.69432	-1.43652
10	1705598408	9.93594	-0.69432	-1.43652
11	1705598409	9.93594	-0.69911	-1.36948
12	1705598411	9.93594	-0.69911	-1.36948
13	1705598412	9.93594	-0.69911	-1.36948
14	1705598413	9.93594	-0.69911	-1.36948
15	1705598415	9.95988	-0.69911	-1.36948
16	1705598416	9.95988	-0.71347	-1.40300

Table 2. Collapse dataset sample.

N°	Timestamp in s	accX in m/s²	accY in m/s²	accZ in m/s²
0	1705673160	9.96467	-0.11492	0.67038
1	1705673162	9.96467	-0.10534	0.67038
2	1705673163	9.96467	-0.10534	0.67038
3	1705673164	9.96467	-0.10534	0.67038
4	1705673166	9.96467	-0.10534	0.67038
5	1705673167	9.96946	-0.10534	0.67038
6	1705673168	9.96946	-0.09577	0.67038
7	1705673170	9.96946	-0.09577	0.68474
8	1705673171	9.96946	-0.09577	0.68474
9	1705673172	9.96946	-0.09577	0.68474
10	1705673174	9.96946	-0.09577	0.68474
11	1705673175	10.96946	-0.80534	0.98474
12	1705673176	9.96946	-0.70534	0.65601
13	1705673178	10.96946	-0.10534	1.95601
14	1705673179	10.96946	-0.90534	0.65601
15	1705673180	9.96946	-0.10534	0.65601
16	1705673182	9.95030	-0.10534	0.65601
17	1705673183	11.9503	-0.19492	1.85601
18	1705673184	10.09504	-0.31492	0.95601

[1] The vertical axis is X

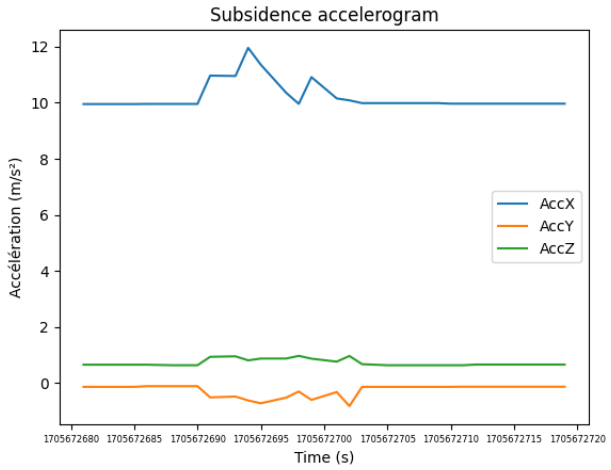

Figure 12. Collapse accelerogram.

Table 3. Subsidence dataset sample.

N°	Timestamp in s	accX in m/s²	accY in m/s²	accZ in m/s²
0	1705672681	9.95030	-0.13408	0.65601
1	1705672682	9.95030	-0.13408	0.65601
2	1705672684	9.95030	-0.13408	0.65601
3	1705672685	9.95030	-0.13408	0.65601
4	1705672686	9.95509	-0.11013	0.65601
5	1705672688	9.95509	-0.11013	0.63686
6	1705672689	9.95509	-0.11013	0.63686
7	1705672690	9.95509	-0.11013	0.63686
8	1705672691	10.96501	-0.51012	0.93682
9	1705672693	10.95202	-0.48013	0.95476
10	1705672694	11.95601	-0.61971	0.81126
11	1705672695	11.35501	-0.71971	0.87516
12	1705672697	10.35502	-0.51971	0.87516
13	1705672698	9.95709	-0.29971	0.97112
14	1705672699	10.91102	-0.59971	0.87112
15	1705672701	10.15109	-0.31971	0.76516
16	1705672702	10.08382	-0.81971	0.96716
17	1705672703	9.98382	-0.13408	0.67516

for the offset elimination and the low-pass filter bandwidth set at 21 Hz to smooth the signal by removing the high-frequency noise. Therefore, the data presents a type A uncertainty assessed on the non-event data: accX = ±0.0108, accY = ±0.0103, and accZ = 0.0206 respectively, computed using the standard deviation metric.

In order to make difference between phenomena and generate eventual alerts, we have opted for three types of tests that could help to make difference between two acquired signals and probably help to use machine learning algorithm to classify if needed. The assessment consists in comparing different signals to the reference signal (which is the non-event signal).

The aim of the two first tests: Cross-correlation and spectral matching, is to give a sneak peek of how data can be differentiated in order to generate accurate alerts. And the third test PCA: tend to show how this data can be prepared to be used with machine learning algorithm.

Test 1: Cross correlation

The relationship between two random signals may be analysed by the cross-correlation [26]. Cross-correlation (also called cross-covariance) between two input signals is a kind of template matching. Cross-correlation can be done in any number of dimensions. [27]. The interpretation of this metric is based on the value of the correlation coefficient:

- If signals are correlated, $r = +1$,
- If signals are not correlated, $r = 0$,
- If signals are opposites, r=-1.

For this study, we have achieved the correlation test using Matlab software.

First, we submit the non-event signal, and the collapse ones to the cross correlation. This yield: a correlation coefficient $r = 0.4294$ and is approaching 0, that is to say these two signals are different.

Secondly, we compare the non-event signals, and the subsidence ones, hence: with a correlation coefficient $r = 0.16857$ lesser than 1 that denotes the big difference between these two signals.

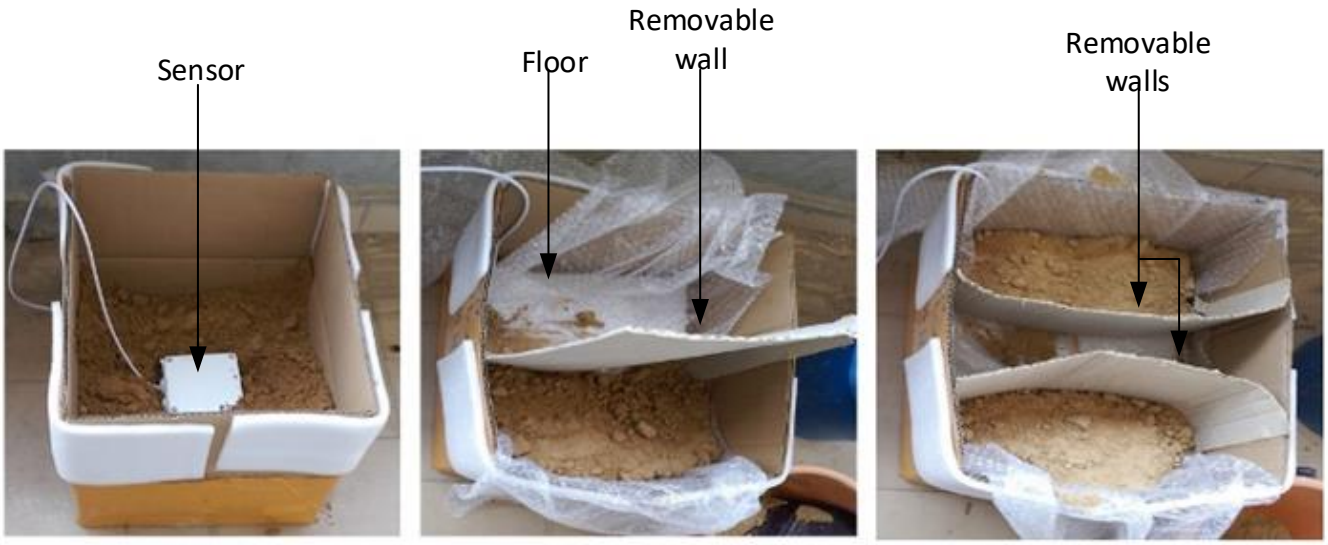

Figure 13. Experimental setup presentation. The IMU sensor planted on the bottom of the simulation bag (left); collapse phenomenon simulation when pulling up the middle gate (central); subsidence phenomenon simulation when pulling up both gates (right).

Test 2: Spectral matching

In this test, we are using the power spectral density or autospectrum. The power spectral density is a real non-negative and even function of frequency and it can be used instead of the autocorrelation function when one wants, for instance, to discover if there are several periodic signals masked by noise. [26].

We have achieved this present test by means of the python programming language.

First, the non-event signals, and the collapse ones (Figure 14). With:

- Spectral distance between the two signals according to X: 0.24188718123466746;
- Spectral distance between the two signals according to Y: 0.3674877256068698;
- Spectral distance between the two signals according to Z: 0.5853259392271702.

Considering the Figure 14, and the different distances values so we establish the difference between these two signals.

Secondly, the non-event, and the subsidence signals (Figure 15). With:

- Spectral distance between the two signals according to X: 0.8800078531203375;
- Spectral distance between the two signals according to Y: 0.839084684286242;
- Spectral distance between the two signals according to Z: 0.29927907274054166.

Considering the Figure 15, with the different distances values we establish the difference between these two signals.

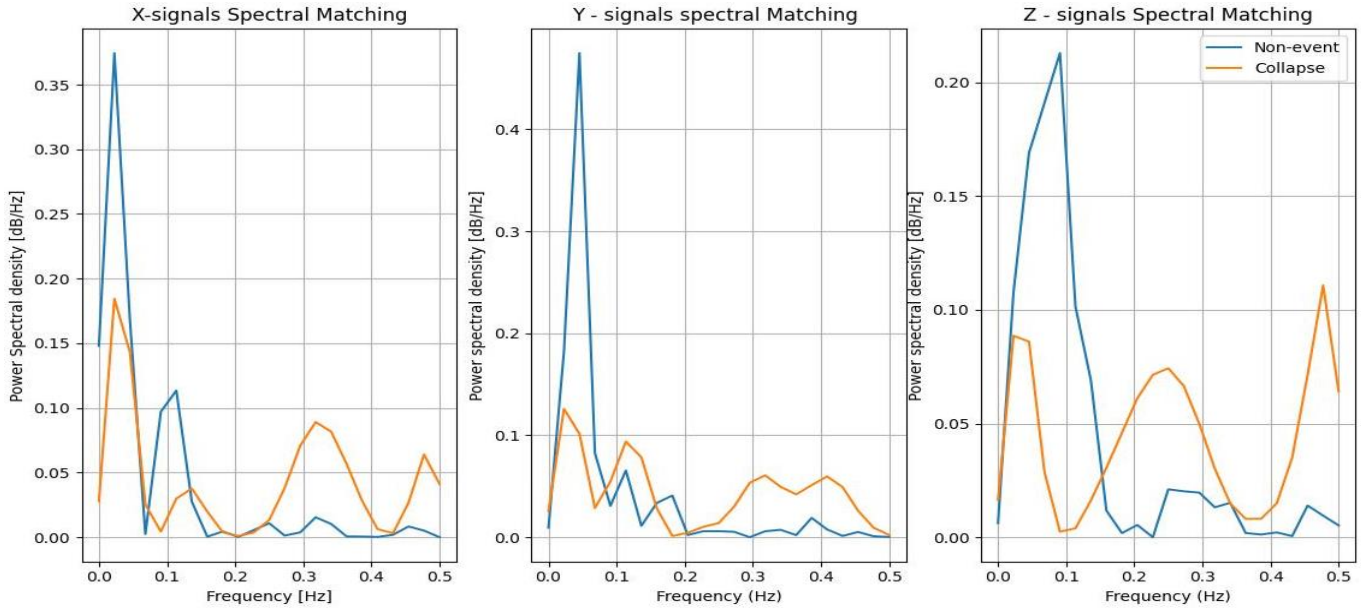

Figure 14. Spectral matching between non-event and Collapse event.

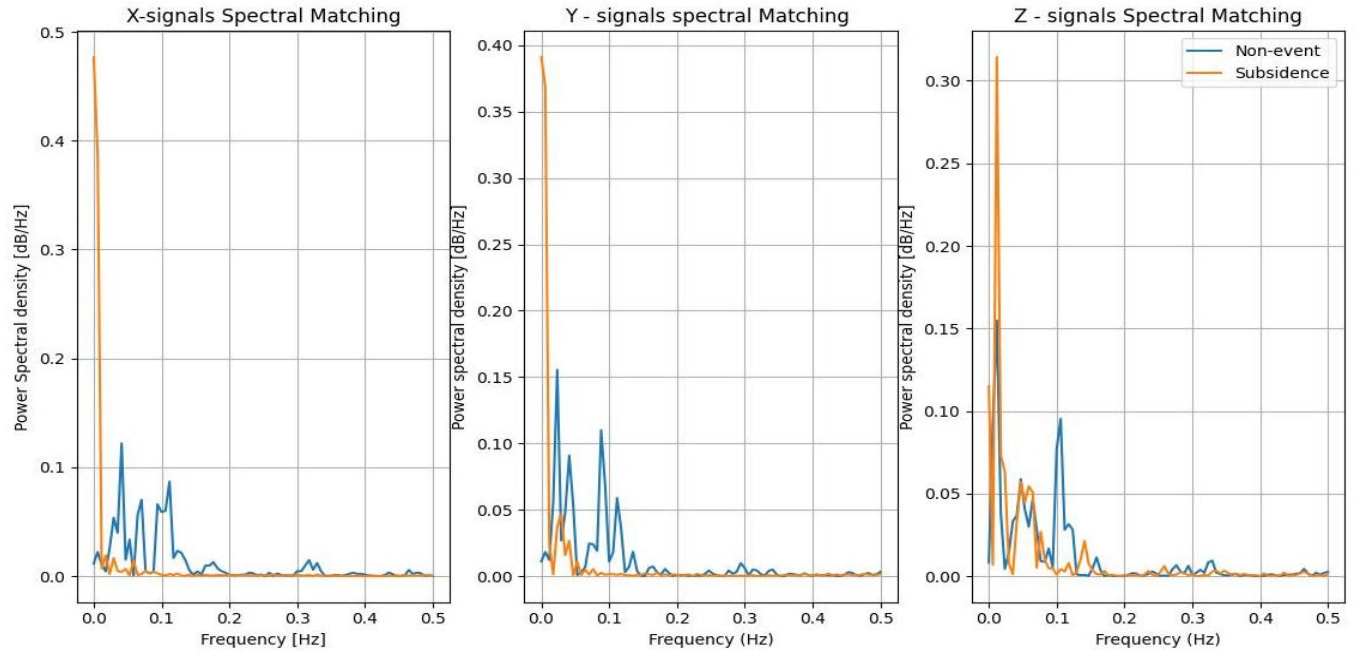

Figure 15. Spectral matching between Non-event, and Subsidence

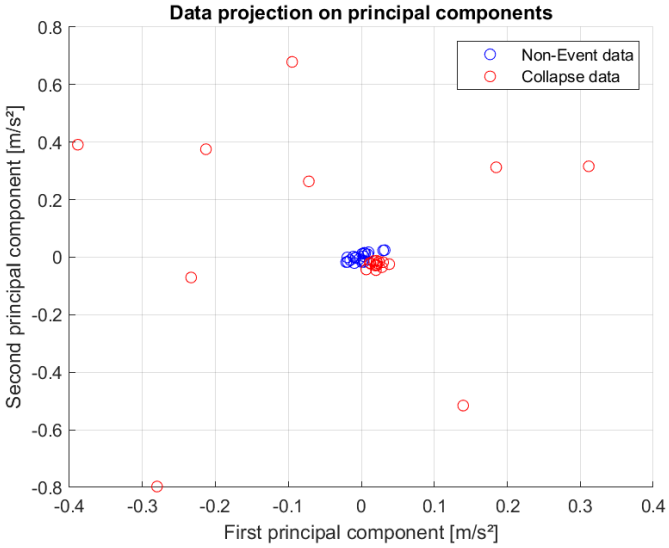

Figure 16. Non-event, and collapse PCA.

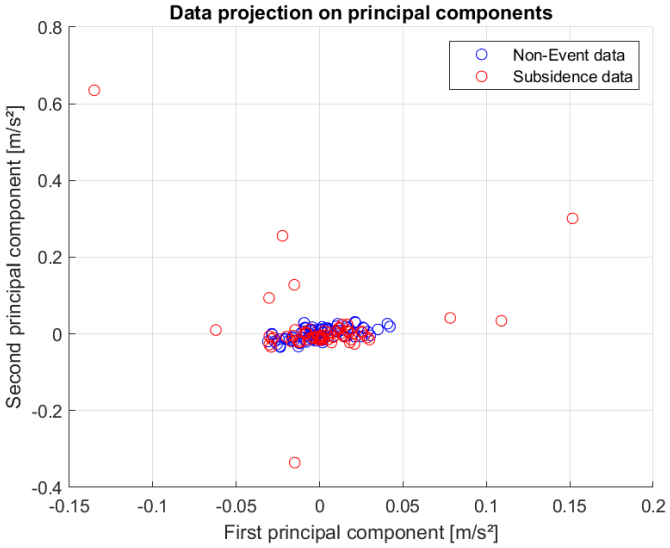

Figure 17. Non-event, and subsidence PCA.

Test 3: Principal Component Analysis

Principal component analysis is a method that rotates the dataset in a way such that the rotated features are statistically uncorrelated after that a subset of the new features could be selected, according to how important they are for explaining the data. [28].

We have used the software Matlab to achieve these tests.

First, between the non-event signals, and the collapse ones and got the output of Figure 16.

The interpretation of this test consists in the overlap between the blue, and the red points show the similitude between the two signals, and the disparity of the red point show the difference between these two signals.

Secondly, between the non-event, and the subsidence signals.

As for the previous case, the difference between these two signals is shown by the spreading of red points on the figure.

For these two experiences: that is, comparing the collapse and subsidence data to the non-event data, we have that the two classes separate quite well in the two-dimensional space. This leads us to believe that even a linear classifier (that would learn a line in this space) could do a reasonably good job at distinguishing the two classes.

For these three tests, we recommend the use of the two first in the case of the alert generation because these are the one which provide a numbered result. In order to build an efficient system in life size, we have to apply these processing tools to real signals of the site in order to define the threshold that allows to generate alerts.

And to perform a machine learning model we recommend the use of the PCA and then a linear classifier (for example: k-Neighbors classifiers, Neural Network, Tree decision, …).

5. CONCLUSION

In this paper, we have assessed the potential of wireless multiparametric (accelerometer, gyroscope, and the integrated onboard temperature sensor) sensors for application to the ground movement detection (and prediction) compared to three more used methods (seismic monitoring, GBRAR, and GBSAR) this yield to the promising results in feasibility, efficiency and implementation cost as shown at section 3 and 4, and also the ease of complementarity with others detection methods.

Some considerations are made for the simulation sake, namely, the small mass of the soil used to perform the simulation of the collapse, and the subsidence, that is why we have not considered the peaks values of the accelerations on different axis.

From this result, it is clear to determine the abnormal movement apparition, but to determine which kind of movement it is (collapse or subsidence), we have to use an enormous dataset in order to define the threshold of the spectral distance between signals to handle the alert, for example using the spectral matching.

In life size, the implementation of the system will depend on the accelerometric values of the site to auscultate, and this related to the soil type, to the current solicitation type, and to the recurrent movement on this site.

As future perspective, with this system we can perform other functionalities like movement prediction, identification of the type of the ground movement (collapse or subsidence), … if we can build a dataset, and apply artificial intelligence algorithms to the concerned site data.

REFERENCES

[1] A. Dauphiné, D. Provitolo, Risques et catastrophes. Observer, spatialiser, comprendre, gérer. Armand Colin, Paris, 2013, 2nd edition, ISBN-13 978-2200278427, 426 pp. [in French]

[2] A. Gruzelle, S. Lebaut, An approach to landslide risk analysis and diagnosis: from identification to proactive action, 2022, Volume 17. Online [Accessed 23 December 2023] https://journals.openedition.org/physio-geo/14697

[3] European Commission. SAFELAND: Living with Landslide Risk in Europe; Assessment, Effects of Global Change, and Risk Management Strategies. Final Report Summary, 2013, CORDIS - EU Research Results. Online [Accessed 11 January 2024] https://cordis.europa.eu/publication/rcn/15870_en.html

[4] X. Fan, G. Scaringi, O. Korup, A. J. West, C. J. V. Western, H. Tanyas, N. Hovius, T. C. Hales, (+ 9 more authors), Earthquake-induced chains of geologic hazards: patterns, mechanisms, and impacts. Reviews of Geophysics, (2019), vol. 57, no. 2, p. 421-503. DOI: 10.1029/2018RG000626

[5] D. Petley, Global patterns of loss of life from landslides, Geology, 2012-b, vol. 40, no. 10, p. 927-930. DOI: 10.1130/G33217.1

[6] D. Petley, Proper investment in large-scale natural hazards research. The Landslide Blog, 2012. Online [Accessed 11 January 2024]

The need for investment in large-scale natural hazards research programmes - The Landslide Blog - AGU Blogosphere
[7] A. Slimi, J. P. Larue, Réseau routier et risque d'éboulements rocheux et de chutes de blocs - cas du tronçon de la route nationale n°5 dans les gorges de Lakhdaria (basse vallée de l'Isser, Bouira, Algérie), Geomaghreb, n°11, 2015, pp. 39-59. [in French]
[8] M. V. Ramesh, D. Pullarkatt, T. H. Geethu, P. V. Rangan, wireless sensor networks for early warning of landslides: experiences from a decade long deployment, 4th World Landslide forum Ljubljana, SlLOVENIA, EU, 29 May - 2 June 2017.
DOI: 10.1007/978-3-319-53487-9_4
[9] C. Bourdeau. Supervision of slopes and unstable cliffs: Design and implementation of the devices of measure - Acquisition and data processing. French Institute of Sciences, and Technologies of Transport, Planning and Networks - IFSTTAR, Techniques and methods, 2016, pp. 32-38.
[10] R. Iannucci, L. Lenti, S. Martino, Seismic monitoring system for landslide hazard assessment and risk management at the drainage plant of the Peschiera Springs (Central Italy), Engineering Geology, Volume 277, November 2020, 105787.
DOI: 10.1016/j.enggeo.2020.105787
[11] J. A. Jornet-Monteverde, J. J. Galiana-Merino, J. L. Soler-LIorens, Design and implementation of a wireless sensor network for seismic monitoring of buildings, Sensors, 2021, 21(11), 3875.
DOI: 10.3390/s21113875
[12] A. Patri, S. P. Rath, S. Jayanthu, Wireless monitoring system for prediction of ground movements in underground mines- a critical review, MineTech 13, The Indian Mining & Engineering Journal, 2013.
DOI: 10.13140/2.1.3471.7122
[13] H. McCormack, A. Thomas, I. Solomon, The capabilities and limitations of satellite InSAR and terrestrial radar interferometry, Fugro NPA Limited, United Kingdom, 2011.
[14] Aurélie Pourrain, Pré-étude de la surveillance des mouvements de terrain en Savoie par série temporelle d'images radar à synthèse d'ouverture Sentinel-1 (imagerie SAR). Architecture, aménagement de l'espace, 2020, dumas-02965838. [in French]
[15] A. Tonnellier, Seismic monitoring of landslides in clay-marl rocks: detection and identification of sources involved in the progression of landslides, Thesis, University of Strasbourg, 2012.
[16] I. Benkechkache, Investigation de la degradation du cadre bati sous l'effet du glissement de terrain cas de Constantine, Université Mentouri de Constantine, 2012, 12 pp. [in French]
[17] Museum of seismology, and geophysics collections, Seismic waves. Online [Accessed November 21, 2023] http://musee-sismologie.unistra.fr/comprendre-les-seismes/notions-pour-petits-et-grands/notions- de-basic/seismic-waves/
[18] J. Burjánek, V. Gischig, J. Moore, and D. Fäh, Ambient vibration characterization and monitoring of a rock slope close to collapse. Geophysical Journal International, (2017).
DOI: 10.1093/gji/ggx424
[19] R. Lannucci, S. Martino, A. Paciello, S. D'Amico, & P. Galea, Investigation of cliff instability at Għajn Ħadid Tower (Selmun Promontory, Malta) by integrated passive seismic techniques. Journal of Seismology, (2020), pp. 1-20.
DOI: 10.1007/s10950-019-09898-z
[20] C. Levy, D. Raucoules, M. Delatre, M. Foumelis, Cross-studies of the hazard of large mass landslides in an urban context (BONIFACIO citadel): contributions of seismic listening techniques, ground radar interferometry and satellite interferometry. Specificity of passive seismic monitoring in Peninsula for the study of rockfall hazard, 2020, pp. 2-3.
[21] C. Negulescu, G. Luzi, M. Crosetto, D. Raucoules, A. Roullé, D. Monfort, L. P. Beneit, (+ 2 more authors), Comparison of seismometer and radar measurements for the modal identification of civil engineering structures, Engineering Structures, 2013, p. 5.
DOI: 10.1016/j.engstruct.2013.01.005
[22] B. Hosseiny, J. Amini, H. Aghababaei, Structural displacement monitoring using ground-based synthetic aperture radar, International Journal of Applied Earth Observation and Geoinformation, (2023).
DOI: 10.1016/j.jag.2022.103144
[23] N. Teppe, Conception et realization d'un démonstrateur embarqué de traitement du signal avec réseau de capteurs sans fils, Electronic, 2013, dumas-01245413. [in French]
[24] S. Crequy, Accelerometric analysis for performance optimization, and risk prevention in cycling, Thesis, University of Reims Champagne-Ardenne, 2015.
[25] P. Masson, éléments de robotique avec Arduino: Accéléromètre, Ecole Polytechnique Universitaire de Nice Sophia-Antipolis, notes de cours (2019), pp. 28-36. [in French]
[26] D. A. Lyon, The discrete fourier transform, part 6: cross-correlation, Journal of Object technology, 2010, vol. 9, No. 2.
DOI: 10.5381/jot.2010.9.2.c2
[27] A. F. Kohn, Autocorrelation and Cross-Correlation Methods. In: Wiley Encyclopedia of Biomedical Engineering, Ed. Metin Akay, Hoboken: John Wiley & Sons, (2006), ISBN: 0-471-24967-X, pp. 260-283.
[28] A. C. Müller, S. Guido, Introduction to Machine learning with python: a guide for data scientists, O'REILLY Media, Sebastopol, 2016, ISBN: 978-1-449-36941-5, 140.